HHS Public Access

Author manuscript

Cell Calcium. Author manuscript; available in PMC 2017 June 02.

Published in final edited form as:

Cell Calcium. 2012 January ; 51(1): 22–30. doi:10.1016/j.ceca.2011.10.002.

Identification of a disulfide bridge essential for structure and function of the voltage-gated Ca^{2+} channel $\alpha_2\delta$-1 auxiliary subunit

Aida Calderón-Rivera[a,1], **Arturo Andrade**[b,1], **Oscar Hernández-Hernández**[c], **Ricardo González-Ramírez**[d], **Alejandro Sandoval**[e], **Manuel Rivera**[f], **Juan Carlos Gomora**[f], and **Ricardo Felix**[a,*]

[a]Department of Cell Biology, Center for Research and Advanced Studies of the National Polytechnic Institute (Cinvestav-IPN), Mexico City, Mexico

[b]Department of Neuroscience, Brown University, Providence, RI, USA

[c]Department of Genetics, National Institute of Rehabilitation (INR), Mexico City, Mexico

[d]Department of Molecular Biology and Histocompatibility, "Dr. Manuel Gea González" General Hospital, Ministry of Health, Mexico City, Mexico

[e]School of Medicine FES Iztacala, National Autonomous University of Mexico (UNAM), Tlalnepantla, Mexico

[f]Departamento de Neuropatología Molecular, Instituto de Fisiología Celular, UNAM, Mexico City, Mexico

Abstract

Voltage-gated calcium (Ca_V) channels are transmembrane proteins that form Ca^{2+}-selective pores gated by depolarization and are essential regulators of the intracellular Ca^{2+} concentration. By providing a pathway for rapid Ca^{2+} influx, Ca_V channels couple membrane depolarization to a wide array of cellular responses including neurotransmission, muscle contraction and gene expression. Ca_V channels fall into two major classes, low voltage-activated (LVA) and high voltage-activated (HVA). The ion-conducting pathway of HVA channels is the α_1 subunit, which typically contains associated β and $\alpha_2\delta$ ancillary subunits that regulate the properties of the channel. Although it is widely acknowledged that $\alpha_2\delta$-1 is post-translationally cleaved into an extracellular α_2 polypeptide and a membrane-anchored δ protein that remain covalently linked by disulfide bonds, to date the contribution of different cysteine (Cys) residues to the formation of disulfide bridges between these proteins has not been investigated. In the present report, by predicting disulfide connectivity with bioinformatics, molecular modeling and protein biochemistry experiments we have identified two Cys residues involved in the formation of an intermolecular disulfide bond of critical importance for the structure and function of the $\alpha_2\delta$-1 subunit. Site directed-mutagenesis of Cys404 (located in the von Willebrand factor-A region of α_2) and Cys1047 (in the extracellular domain of δ) prevented the association of the α_2 and δ peptides upon proteolysis, suggesting that the mature protein is linked by a single intermolecular

*Corresponding author at: Departamento de Biología Celular, Cinvestav-IPN, Avenida IPN #2508, Colonia Zacatenco, México D.F., CP 07300, México. Tel.: +52 55 57 47 39 88; fax: +52 55 57 47 33 93. rfelix@cell.cinvestav.mx (R. Felix).

[1]These authors contributed equally to this work.

disulfide bridge. Furthermore, co-expression of mutant forms of $\alpha_2\delta$-1 Cys404Ser and Cys1047Ser with recombinant neuronal N-type ($Ca_V2.2\alpha_1/\beta_3$) channels, showed decreased whole-cell patch-clamp currents indicating that the disulfide bond between these residues is required for $\alpha_2\delta$-1 function.

Keywords

Calcium channels; $\alpha_2\delta$ Subunit; Disulfide bonds; Calcium channel structure

1. Introduction

Calcium is an essential and versatile intracellular messenger. Normally submicromolar levels of Ca^{2+} within the cytoplasm are disrupted by Ca^{2+} increases that trigger diverse Ca^{2+}-dependent responses [1]. Transient increases in cytosolic Ca^{2+} can be the result of entry from the extracellular space or release from intracellular stores. Ca^{2+} influx may be mediated by several molecules [1], including voltage-gated (Ca_V) channels which have been subdivided according to their activation threshold into (i) low voltage-activated (LVA or T-type) channels and (ii) high voltage-activated (HVA) channels, a class that includes the L-, N-, P/Q- and R-types [2,3]. Biochemical purification has revealed that HVA channels are composed of four proteins, including the pore-forming α_1 and auxiliary $\alpha_2\delta$, β and γ subunits [3–5].

The $\alpha_2\delta$ subunit is a protein of ~170 kDa encoded by a single gene that is translated as a precursor polypeptide. The δ domain anchors the α_2 protein to the cell membrane via a single putative transmembrane segment. The α_2 domain is entirely extracellular [3,5–7], is heavily glycosylated and contains several functional domains. These include a ~180 amino acid von Willebrand factor-A (vWFA) domain similar to extracellular matrix-binding regions of integrins, a 5 amino acid metal ion-dependent adhesion site (MIDAS) motif [8] and a poorly understood 92 amino acid Cache (Ca^{2+} channels, chemotaxis receptors) domain. The transmembrane segment of δ and some extracellular regions of α_2 are thought to associate with the α_1 subunit [9].

Even though the physiological relevance of $\alpha_2\delta$ is not well defined, there is evidence indicating a role in trafficking and also in the modulation of Ca_V channel properties. Heterologous expression of $\alpha_2\delta$ with various α_1 and β subunits results in an increase in current density, acceleration of current activation and inactivation and hyperpolarizing shifts in the current–voltage relationship [5–7]. The mechanisms for these effects are as yet incompletely defined, although the increase in current density could be explained by improved targeting of Ca_V channels to the plasma membrane [8,10] and significant reduction in the rate of entry of surface resident channels into degradative pathways [11]. Additionally, Ca_V channels appear to be segregated into cholesterol-rich membrane microdomains (i.e. lipid rafts), and it has been found that the $\alpha_2\delta$ subunit is necessary and sufficient for targeting channels to lipid rafts [12,13].

Four subtypes of the $\alpha_2\delta$ protein (1–4) encoded by four separate genes with several known splice variants have been described [3,5–7]. Interestingly, some insights into the functional

role of the $\alpha_2\delta$ auxiliary subunits *in vivo* come from a series of spontaneously occurring mutations in mice. For example, mutations in $\alpha_2\delta$-2 (ducky, entla) that result in similar phenotypes characterized by ataxia, paroxysmal dyskinesia, and spike wave seizures [14–16], and mutations in $\alpha_2\delta$-4 that presumably underlies a channelopathy that leads to cone-rod dysfunction in the murine visual system [17]. Last, $\alpha_2\delta$-1 and $\alpha_2\delta$-2 subunits have been shown to be a target of gabapentinoid drugs, which are small molecules with anticonvulsant and analgesic effects that exert chronic inhibitory actions on Ca_V channel functional expression [16,18–22], although the role of $\alpha_2\delta$ in epilepsy and neuropathic pain remains unclear.

As mentioned earlier, during biosynthesis $\alpha_2\delta$ subunits are generated as large precursor proteins, which undergo posttranslational cleavage, oxidation and glycosylation to yield mature proteins comprised of disulphide-linked α_2 and δ glycopolypeptides [3,5–7,23,24]. Although we have learned much about the posttranslational modification of $\alpha_2\delta$ [23–26] the precise role of these events for Ca_V channel function is only partially understood. In particular, the exact role of disulphide bonding between α_2 and δ has not been well established and the exact cysteine residues involved in this intermolecular interaction are unknown. Therefore, in the present study, we aimed to identify the residues responsible for the disulfide bridging in the $\alpha_2\delta$ auxiliary subunit.

2. Materials and methods

2.1. Cell culture and transfection

Human embryonic kidney (HEK) 293 cells (ATCC, Manassas, VA) were maintained in Dulbecco's modified essential medium-high glucose supplemented with 10% horse serum, 1% L-glutamine, 110 mg/L sodium pyruvate and antibiotics, at 37 °C in a 5% CO_2-95% air humidified atmosphere. Gene transfer was performed using Lipofectamine Plus reagent (Invitrogen, Carlsbad, CA). Briefly, for a 35-mm Petri dish of HEK293 cells, 2 μg of the plasmid cDNA encoding the rabbit brain N-type Ca^{2+} channel $Ca_V2.2$ pore-forming subunit (GenBank accession number D14157) [27]; in combination with 2 μg cDNA of the rat brain β_3 (M88751) [28]; and 2 μg cDNA coding the wild-type rat brain $\alpha_2\delta$-1b cDNA (M86621) [29]; or its mutants were premixed with 6 μL of Lipofectamine in 100 μL serum-free medium according to the manufacturer's instructions. The solution was then added to the dish and cells grown at 37 °C for 24 h, when medium was changed. The $Ca_V2.2\alpha_{1B}/\alpha_2\delta$-1b/$\beta_3$ subunit composition was selected to emulate the structure of the native N-type Ca^{2+} channels [30–32].

2.2. Site directed mutagenesis

The $\alpha_2\delta$-1 cDNA was inserted into the recombinant bicistronic expression plasmid pIRES-hr-GFP1A [23,24] and expressed under the control of a cytomegalovirus promoter. The point mutations were introduced with ~40-mer synthetic oligonucleotides using the Quik-Change XL-mutagenesis kit (Stratagene, La Jolla, CA). Initially, single amino acid mutations changing a cysteine residue to a methionine or serine were created. Next, multiple mutations were done using suitable mutagenic primers. cDNAs of all mutant channel $\alpha_2\delta$-1 subunit

were sequenced on an automated sequencer ABIPrism310 (PerkinElmer Applied Biosystems, Foster City, CA).

2.3. Electrophysiology

Ionic currents from HEK293 cells were recorded at room temperature (~22 °C) using the whole-cell configuration of the patch-clamp technique [33] 48 h after transfection. Ba^{2+} was used as the charge carrier. The extracellular solution contained (in mM): $BaCl_2$, 10; TEA-Cl, 125; HEPES, 10; glucose, 10 (pH 7.3). The intracellular solution contained (in mM): CsCl, 110; $MgCl_2$, 5; EGTA, 10; HEPES, 10; Na-ATP, 4; GTP, 0.1 (pH 7.3). Recordings were performed using an Axopatch 200B amplifier (Axon Instruments, Foster City, CA). Currents were digitized at a sampling rate of 5.7 kHz and filtered at 2 kHz (four-pole Bessel filter). Linear leak and parasitic capacitance components were subtracted on-line using a P/4 protocol. Membrane capacitance (C_m) was determined as previously described [34] and used to normalize currents.

Current–voltage (I–V) relationships were obtained by step depolarization between −50 mV and +60 mV in 10 mV increments, from a typical holding potential (V_h) of −80 mV. To assess steady-state inactivation properties, a 1-s conditioning pulse to various holding potentials preceded a test depolarization to +10 mV. The peak current values were converted to peak conductance values using the expression $G = I/(V_m - V_{rev})$, where I is current, G is conductance, V_m is the test potential and V_{rev} is the extrapolated reverse potential. Conductance–voltage (G–V) curves for activation were fit with a Boltzmann equation of the form $G = G_{max}/(1 + \exp[(V_m - V_{1/2})/k]^{-1})$, where G_{max} is maximum conductance, V_m is the test potential, $V_{1/2}$ is the potential for half-maximal activation of G_{max} and k is a slope factor. Steady-state inactivation curves were fitted with a Boltzmann function $I_{Ba} = I_{max}/(1 + \exp[(V_m - V_{1/2})/k])$, where the current amplitude I_{Ba} has decreased to a half-amplitude at $V_{1/2}$ with an e-fold change over k mV. Time-to-peak (TtP) was measured using a trough-seeking function in pClamp within the test pulse duration. Current remaining was measured from an average of three individual sweeps per recording using the equation: $I_{rem} = 100 \times (I_{end}/I_{peak})$, where I_{rem} is the current remaining at the end of a 140-ms test pulse, I_{end} is the value at the end of the test pulse, and I_{peak} is the maximum inward current measured during the test pulse.

2.4. SDS-PAGE and western blotting

Microsomes from transfected HEK293 cells were prepared as previously described [25,35]. Briefly, cells were harvested, washed twice with PBS and homogenized during 15 min in cold lysis buffer (50 mM Tris–HCl [pH 7.4], 0.8 μM aprotinin, 640 μM benzamidin, 1.1 μM leupeptin, 0.7 μM pepstatin and 230 μM PMSF). Homogenized was clarified at 3000 rpm/4 °C during 5 min. After centrifugation at 38,000 rpm/4 °C during 37 min pellet was suspended in sucrose buffer (0.3 M sucrose, 20 mM Tris–HCl [pH 7.4] and protease inhibitors) and stored at −70 °C. SDS-PAGE analysis was performed under reduced or non-reduced conditions as follows. Aliquots of 100 μg of protein were mixed with sample buffer (50 mM Tris–HCl [pH 6.8], 1.7% SDS, 5% glycerol, 0.002% bromophenol blue) containing or not the reducing agent dithiothreitol (DTT) at 100 mM and boiled for 5 min. Samples were subjected to 8% SDS-PAGE electrophoresis. After electrophoresis, proteins were

transferred to a nitrocellulose membrane (Hybond-N; GE Healthcare, Buckinghamshire, UK). After blocking with non-fat milk (5%) supplemented with 0.2% Tween 20, membranes were incubated overnight with the primary anti $\alpha_2\delta$-1 antibody 1:200 in TBS-T with 5% non-fat milk (Alomone labs, Jerusalem, Israel) washed in TBS-T (10 mM Tris–HCl, 0.15 M NaCl, 0.05% Tween 20), incubated with horseradish peroxidase goat anti-rabbit secondary antibody and developed with the Amersham ECL reagent according to the manufacturers' instructions.

2.5. Bioinformatics

Multiple protein sequences were aligned using the modified Clustal W algorithm [36] of Vector NTI 8 software package (Invitrogen). The disulfide bonds prediction was performed using DiAminoacid Neural Network Application (DiANNA 1.1), which is a recent state-of-the-art web-based software determining the cysteine oxidation state and disulfide connectivity of a protein [37,38] available at http://clavius.bc.edu/(clotelab/DiANNA/. Bonds with a score >0.9 were considered for further analysis. Homology modeling was performed by analyzing the α_2 and the δ domains separately. The sequence from residues 1–944 (α_2) and 945–1091 (δ) were modeled by the Robetta [39] and the I-TASSER [40] full-chain protein structure prediction servers (http://robetta.bakerlab.org and http://zhanglab.ccmb.med.umich.edu/I-TASSER, respectively). Models were assessed using Swiss-Model server and visualized using the Chimera package available from the Resource for Biocomputing, visualization and Informatics at UCSF (http://www.cgl.ucsf.edu/chimera).

3. Results

As a first step to identify the molecular determinants of the interchain disulfide bond(s) between the two domains of the Ca_V channel $\alpha_2\delta$-1 auxiliary subunit, we searched for conserved cysteine residues in the protein using multiple sequence alignments. Since the α_2 domain is a 944 amino acid polypeptide characterized by a large number of cysteine residues, we decided to start our analysis by performing the sequence alignment on the extracellular region of the δ domain, a 117 amino acid region that showed to possess only six conserved Cys. A selection of the δ peptide sequences aligned to show the pattern of the Cys residues is shown in Fig. 1A.

We next investigated the functional role of the six conserved Cys in the extracellular region of δ by preparing single mutant variants. Initially, we constructed the Cys962Met mutation to preserve the sulfur atom in the amino acid. However, changing a hydrophilic residue by a more hydrophobic one could alter the properties of the protein, and therefore the rest of the conserved Cys were replaced by serine (Ser) residues (Fig. 1B). This change produces a smaller structural alteration and is likely to maintain the polarity and size of the amino acid side chains as close as possible to the original protein. The mutants were then transiently co-expressed with the N-type ($Ca_V2.2$) HVA channel α_1 pore-forming and the β_3 auxiliary subunit in HEK293 cells, and whole-cell patch clamp recording was then used to examine the effects of the mutations on functional channel expression. Inward Ba^{2+} current (I_{Ba}) through Ca_V channels containing the wild-type (WT) $\alpha_2\delta$-1 auxiliary subunit displayed the

hallmark characteristics of $\alpha_2\delta$-mediated channel regulation such as increased current density and hyperpolarizing shifts in the voltage dependences of activation and inactivation, and acceleration of inactivation kinetics (Figs. 2 and 3). Interestingly, when examining current densities obtained in the presence of WT and mutant subunits, five out of the six Cys mutants showed no loss of $\alpha_2\delta$-mediated regulation (Fig. 1B). In sharp contrast, a subsequent electrophysiological analysis using the same protocol showed that the degree of current upregulation was significantly less than that of WT when the Cys1047Ser mutant was co-expressed with the N-type ($Ca_V2.2\alpha_1/\beta_3$) channel (Fig. 2A).

To further characterize the role of Cys1047, additional multiple mutants of the $\alpha_2\delta$-1 subunit containing the Cys1047Ser mutation along with Cys962Met, Cys984Ser, Cys987Ser, Cys1032Ser and Cys1059Ser substitutions (C5 and C6) were engineered and co-expressed with the N-type ($Ca_V2.2\alpha_1/\beta_3$) channel. As expected, neither of the latter mutations resulted in the upregulation of current density normally observed after co-expression of the WT $\alpha_2\delta$-1 subunit (Fig. 2B) measured at +10 mV. These data thus further support the notion of residue 1047 being a crucial determinant of $\alpha_2\delta$-1 protein modulation of N-type channels. A similar pattern was observed in whole cell recordings from HEK293 cells in experiments where macroscopic currents were evoked by a series of depolarizing steps ranging from −50 mV to +60 mV from a V_h of −80 mV. Mean currents at all command potentials were 2- to 4-fold smaller in cells expressing $\alpha_2\delta$-1 subunits containing the Cys1047Ser mutant compared with cells expressing the WT protein (Fig. 2C). In summary, recombinant N-type ($Ca_V2.2\alpha_1/\beta_3$) channel function was not affected by the substitution of Cys962 by Met or Cys984, 987, 1032, 1059 by Ser in the $\alpha_2\delta$-1 auxiliary subunit, but it was impaired by the substitution of Cys1047 by Ser. Therefore, the later cysteine residue is required for $\alpha_2\delta$-1 function.

The loss of channel function as a result of the Cys1047Ser amino acid substitution could be attributed to different mechanisms that affect channel activity and/or channel membrane expression. To get insight into the effect of this mutation, a kinetic analysis was next performed where we measured the time-to-peak of I_{Ba} and the current remaining (I_{rem}) at the end of the command pulse as indices of channel activation and inactivation, respectively (Fig. 3). *TtP* was measured at a test potential of +10 mV from a V_h of −80 mV. As can be seen in Fig. 3A, *TtP* was significantly slower for currents recorded in cells transfected with $\alpha_2\delta$-1 subunits containing the Cys1047Ser mutation. In addition, mutating the six conserved Cys residues within the extracellular loop of the δ domain or the substitution of the Cys1047 alone affected the voltage dependence of channel activation. Fig. 3C shows that there is an overlap in the activation curves independently of what $\alpha_2\delta$-1 mutant was co-expressed with of $Ca_V2.2\alpha_1/\beta_3$ channels. In contrast, in $Ca_V2.2\alpha_1/\beta_3$ channels containing the WT $\alpha_2\delta$-1 subunit the activation curve appeared shifted 5–10 mV toward more negative potentials, suggesting that Cys1047 within the δ sequence may participate in the $\alpha_2\delta$-mediated regulation of the coupling between the voltage sensor and the channel gate.

The participation of $\alpha_2\delta$-1 in the regulation of Ca_V channel voltage-dependent inactivation is well documented. This auxiliary subunit tends to accelerate inactivation kinetics and produces a hyperpolarizing shift in half-inactivation potential of all Ca_V channels subtypes [35,41,42]. Consistent with this, in the absence of $\alpha_2\delta$-1 the fraction of channels that

inactivated after a 140-ms depolarizing pulse did not exceed 50% over a wide range of voltages, and no negative shifts in half-inactivation potential was observed. In contrast, as seen from the raw current records in Fig. 2A and from the data shown in Fig. 3B, co-expression with $\alpha_2\delta$-1 WT or its mutants resulted in a significant change in the inactivation kinetics of $Ca_V2.2\alpha_1/\beta_3$ channels. It should be noted however, that the percentage of residual current remaining at the end of the pulse was different for channels containing the WT and the Cys1047Ser mutation. The WT $\alpha_2\delta$-1 subunit preferentially accelerated inactivation kinetics of the $Ca_V2.2\alpha_1/\beta_3$ channels, while inactivation kinetics of channels was not effectively regulated by the mutant $\alpha_2\delta$-1 subunits (Fig. 3B). Likewise, Fig. 3D illustrates the steady-state inactivation behavior of the Ca_V channels in the presence of the WT and mutant $\alpha_2\delta$-1 auxiliary subunits. Ca_V channels containing the WT subunit, but not the Cys1047Ser or the C6 mutations, exhibited a discernible ~10 mV hyperpolarizing shift in half-inactivation potential.

To further address the role of the conserved Cys residues within the transmembrane δ domain in the formation of a disulfide bridge within $\alpha_2\delta$-1, the WT auxiliary subunit and its mutated versions were expressed in HEK293 cells and analyzed by immunoblotting. In these experiments, proteins were exposed to a reducing agent (DTT) to disrupt endogenous disulfide bridges between Cys residues. The result of this analysis showed that under non-reducing conditions the WT protein migrates as a high molecular mass protein of ~170 kDa. Given that the epitope recognized by the $\alpha_2\delta$-1 antibody used in these experiments is located in the N-terminal of α_2, upon reduction with DTT the majority of the protein migrated as a product of the predicted size for the α_2 peptide (~140 kDa). This result confirmed that under our experimental conditions the WT $\alpha_2\delta$-1 subunit is proteolytically cleaved into separate α_2 and δ peptides (Fig. 4A). Likewise, expression of the α_2 protein alone (lacking the δ domain) as a control, resulted in the presence of high molecular mass species of ~140 kDa under both reducing and non-reducing conditions, as expected (Fig. 4A).

To confirm that the conserved Cys 962, 984, 987 and 1032 present in the extracellular domain of the δ protein are not involved in disulfide bonding as predicted from the functional data, we compared the mobility of the previously genetically engineered δ single mutants expressed in HEK293 cells with that of the WT $\alpha_2\delta$-1 protein under reducing and non-reducing conditions. As shown in Fig. 4B, single mutants Cys962Met, Cys984Ser, Cys987Ser and Cys1032Ser exhibited an identical mobility pattern as the WT $\alpha_2\delta$-1 protein. This result is consistent with the predicted absence of intermolecular disulfide bridges formed by these Cys residues.

In sharp contrast, expression of the Cys1047Ser and the C6 mutations resulted in proteins which size remained unchanged upon reduction, suggesting that the recombinant proteins harboring a mutation in the Cys residue at position 1047 were not able to form the disulfide bond that maintains the α_2 and the δ peptides linked *in vivo* (Fig. 4C). It should be noted that a small fraction of the C6 mutant $\alpha_2\delta$-1 protein migrated as a diffuse ~170 kDa band under non-reducing conditions, suggesting the formation of aberrant intermolecular disulfide bonds that cause the protein to migrate as diffuse smear. However, the majority of the C6 mutant protein appeared to be the expected ~140 kDa form of the proteins, confirming that

Cys1047 participates in the disulfide bond necessary for covalent assembly of the $\alpha_2\delta$-1 complex.

A bioinformatic study was next conducted using DiANNA 1.1 web server [37,38] to predict the counterpart of the Cys1047 involved in the formation of the disulfide bond occurring in the $\alpha_2\delta$-1 subunit. The result of this analysis showed one cysteine residue at position 404 in the α_2 domain potentially involved in this process (Suppl. Table 1). The multi-sequence alignment (using Vector NTI 8 software) demonstrated that Cys404 is conserved in the three species analyzed (Fig. 5A), which strongly supports the hypothesis of a potential role of this amino acid in the $\alpha_2\delta$-1 disulfide bridge formation.

We then examined the hypothesis that a specific disulfide bond formed by Cys404, located in the von Willebrand factor-A region (vWFA) of α_2 extracellular domain of the protein, could be required to generate and maintain the structure that determines the function of the $\alpha_2\delta$-1 subunit. Hence, whole-cell current recordings were carried out following transient transfection of HEK293 cells with the WT or the mutant Cys404Ser $\alpha_2\delta$-1 cDNA constructs, together with the N-type ($Ca_V2.2$) channel α_1 pore-forming and the β_3 auxiliary subunit. In contrast to the robust currents observed following expression of the WT channels, the Cys404Ser mutant subunit failed to induce the upregulation of channel functional expression observed after co-expression of the $\alpha_2\delta$-1 subunit (Fig. 5B and C).

To confirm the role of the Cys residue at position 404 in the intermolecular disulfide bond formation of $\alpha_2\delta$-1, we examined the electrophoretic mobility characteristics of the Cys404Ser mutant expressed in HEK293 cells. Consistent with the results in Fig. 4, when samples were not treated with the reducing agent, the mobility of the WT $\alpha_2\delta$-1 protein decreased, such that the ~170-kDa band was replaced by a band at ~140 kDa. In contrast, the mobility shift under non-reducing conditions, indicative of the presence of a disulfide bond, was eliminated by mutation of Cys404Ser. As can be seen in Fig. 5D, the apparent molecular mass for the mutant $\alpha_2\delta$-1 protein under both reducing and non-reducing conditions was ~140 kDa. Taken as a whole, these results strongly suggest that Cys404 is capable of interacting with Cys1047 to form a disulfide bond in the Ca^{2+} channel $\alpha_2\delta$-1 auxiliary subunit. Assuming a disulfide bond between Cys1047 and Cys404, we speculated that the mutation of Cys404 should present the same functional phenotype as observed for Cys1047. The results of the functional analysis show that indeed substitution of Cys404 to Ser results in significant changes in *TtP* and voltage dependence of channel activation and steady-state inactivation (Fig. 6), as expected.

Last, to further determine the assignment of these two Cys residues in disulfide bonding, a predicted three-dimensional structure of the $\alpha_2\delta$-1 protein was generated by homology modeling (Fig. 7). Given that the two putative domains of the protein were outside the size and complexity limits of Robetta, development of the $\alpha_2\delta$-1 homology model was an iterative process in which the problem was resolved by analyzing both peptides (α_2 and δ) independently. In the first step, a homology model for the α_2 peptide was generated (Fig. 7A). To this end, fold recognition algorithms provided by the Protein Homology/AnalogY Recognition Engine V 2.0 PHYRE2 available at URL http://www.sbg.bio.ic.ac.uk/phyre2/html/page.cgi?id=index [43] were used to score sequence compatibility of proteins that

incorporate the vWFA domain fold. Hence, suitable templates for modeling of $\alpha_2\delta$-1 vWFA domain (residues Asp253-Leu430) were selected from available structures. The crystal structure of the vWFA region from the I-domains of integrins CD11b and CD11a with Mn^{2+} bound to its metal ion-dependent adhesion site (MIDAS), were the best templates. The three-dimensional structure of the vWFA domain in α_2 is represented by a doubly wound, open, twisted β-sheet flanked by α-helices. The domain adopts a classic α/β Rossmann fold and contains the MIDAS region (Suppl. Figs. 1 and 2).

Another domain found in our prediction was the Cache domain. This region consists of an N-terminal with three predicted strands and a α-helix, and a C-terminal with a strand dyad followed by a relatively unstructured region (Suppl. Fig. 3). The three strands in the N-terminal region of the Cache domain form a sheet analogous to that present in the core of PAS, a multifunctional domain found in *Drosophila* period clock protein, aryl hydrocarbon receptor and single-minded proteins [44].

In the next step, a three-dimensional model for the protein structure of the δ subunit was generated. To this end, the known NMR structure of the plasma membrane sarcolipin was used as template [45] for the putative transmembrane domain of δ, while the rest of the model was generated using the experimental structure of a non-related lipase [46]. The model shows that δ adopts a highly defined α-helical conformation from a Val1062 through a Leu1082. The nine amino acid C-terminal (Val1083 through Trp1091) is mostly unstructured, and N-terminal region is characterized by several turn-and-bend regions (Fig. 7B).

Likewise, to model the α_2 region in complex with the δ domain, the above individual three-dimensional models of the two proteins were assembled together using the protein interfaces surfaces and assemblies (PISA) web server (http://www.ebi.ac.uk/msdsrv/protint/pistart.html). The quality of the final model of the $\alpha_2\delta$-1 complex, as assessed by PROCHECK, Mfold, Qmean, Z score (Suppl. Table 2). Stereochemical main-chain and side-chain parameters were better than those for structures determined at 2 Å and 94.1% of residues of the complex were located in the most energetically favored regions. The Dfire value was −1160.64, which suggest a stable conformational structure. The quality of the final model reflected the quality of the crystal structures used as templates for the modeling, and the final three-dimensional model of the $\alpha_2\delta$-1 subunit is shown in Fig. 7C. Using this model we determined the distance between the residues that participate in the disulfide bond (Fig. 7D). The distance between the two Cys residues at positions 404 and 1047 is 5.28 Å. This measurement is within the range of bond distances for the formation of disulfide bridges [47]. In addition, the analysis by PROCHECK showed that the model has the side-chain environment of these Cys is such that they are conformationally able to permit the disulfide bond to adopt a torsional angle of 90° or −90°.

4. Discussion

The topology of the $\alpha_2\delta$-1 subunit was originally determined for the skeletal muscle variant. Three transmembrane segments were suggested for the protein based on hydropathy and biochemical analyses [48,49]. Later studies using site-directed antibodies revealed that the

$\alpha_2\delta$-1 auxiliary subunit was actually a type I transmembrane (TM) protein with an extracellular α_2 domain anchored to the channel complex by a single membrane-located δ domain [25,50,51]. The early molecular studies also suggested that the α_2 and δ peptides were encoded by a single gene and that the $\alpha_2\delta$ mature protein is post-translationally processed with the formation of disulfide bonds, before proteolytic cleavage into the two peptides. However, the exact cysteine residues involved in the formation of the putative disulfide bonds in the mature protein were not identified.

The main finding of our study, which combines bioinformatics, protein biochemistry and site-directed mutagenesis with molecular modeling and electrophysiological recordings, is that the conserved Cys404 and Cys1047 residues located in the vWFA region of α_2 and the extracellular domain of δ, respectively, form a single intermolecular disulfide bridge obligatory for normal $\alpha_2\delta$-1 subunit function. Hence, we used bioinformatics for predicting Cys residues in δ that might form direct contacts with Cys residues in α_2. These residues were mutated to Ser, and a possible disulfide bond formation between mutated subunits was investigated. Most of the Ser residues introduced into the extracellular domain of δ did not cause a change in the electrophoretic mobility of the protein following *in vitro* reduction of disulfide bonds with DTT. As mentioned earlier, under non-reducing conditions the $\alpha_2\delta$-1 WT protein is a diffuse ~170 kDa band. This band was absent in the presence of DTT, becoming a more discrete band of material that migrated at ~140 kDa. The mutation Cys1047Ser, however, migrated as a protein with an apparent molecular mass of about 140 kDa under both reducing and non-reducing conditions, suggesting a crucial role for this Cys residue in disulfide bond formation. Qualitatively similar results were observed when the conserved Cys residue at position 404 in the α_2 extracellular peptide was mutated to Ser, indicating the formation of a disulfide bond between Cys404 and Cys1047.

The above mentioned mutants were also transiently co-expressed in HEK293 cells, and whole-cell patch clamp recording was then used to examine their effects on functional channel expression. Previous studies in heterologous expression systems have shown that $\alpha_2\delta$-1 increases the maximum conductance of different recombinant $Ca_V\alpha_1/\beta$ channels [3,4,6]. In the present work, we show that whereas there was a ~4-fold increase in current density through $Ca_V2.2\alpha_1/\beta_3$ channels upon co-transfection with WT $\alpha_2\delta$-1, both Cys404Ser and Cys1047Ser mutations had little influence in whole-cell current density, implying that formation of an intra-subunit disulfide bond between these residues is essential for $\alpha_2\delta$-1 functional enhancement of Ca^{2+} currents.

Interestingly, it has been proposed that an important fraction of the $\alpha_2\delta$-2 subunit is not proteolytically processed into the α_2 and the δ peptides when expressed in the HEK293-derived cell line tsA201 [26]. Since it is acknowledged that co-expression of $\alpha_2\delta$-2 increases current density through different types of Ca_V channels [8,52], the possibility exists that cleavage of $\alpha_2\delta$ might not be essential for functional enhancement of currents. Although the discrepancy between this finding and the data obtained for the $\alpha_2\delta$-1 subunit might lie in the lack of sequence similarity between the two $\alpha_2\delta$ variants around the site of proteolysis [24,49], the fact that the protein is correctly processed post-translationally in the cerebellum [26] as well as in a HEK293 cell line stably expressing it [53] suggests that the proteolytically cleaved may be also the active form of the protein.

Last, there is now compelling evidence for a major involvement of the $\alpha_2\delta$-1 subunit for targeting the Ca^{2+} channel complex to lipid rafts [12,13,54]. Although the mechanism for this action remains unclear, $\alpha_2\delta$-1 co-localizes with lipid raft marker proteins when expressed in heterologous systems and is also necessary and sufficient for the targeting of neuronal channels to the rafts [12,13,54]. Recently, a new mechanism has been proposed for Ca_V channel localization to lipid rafts, which also challenges the conventional structural model of the $\alpha_2\delta$-1 subunit. This model suggests that the $\alpha_2\delta$ protein associates with the plasma membrane via a glycosylphosphatidylinositol (GPI) anchor attached to the δ peptide [54]. However, studies by Jones and co-workers [55] have demonstrated more recently that the raft localization of $\alpha_2\delta$-1 is preserved after replacement of the reported GPI anchoring motif with the transmembrane domain of the Type I TM-spanning protein PING. This finding is consistent with the idea that the $\alpha_2\delta$-1 subunit resides in lipid rafts via protein-protein and/or specialized lipidprotein interactions, and argues against any involvement of the putative GPI-anchor mechanism. In line with this, the predicted model for the structure of the δ protein (Fig. 7B) is consistent with a model where the $\alpha_2\delta$-1 subunit retains its type I transmembrane topology. Using a selection of membrane topology prediction methods (Uniprot, MEMSAT-SVM, MEMSAT3 and Kyte-Doolitle) different models were produced for the δ peptide. There was a consensus between all prediction methods that the protein has one TM spanning helix in the region comprising amino acid residues Val1062 through a Leu1082. It is worth emphasizing that final three-dimensional structure presented here for δ (Fig. 7B) is in general agreement with existing experimental data, and that the confidence scores for estimating the quality of the predicted model (Suppl. Table 2), indicate adequate levels of certainty that the templates used were appropriate for modeling the proteins.

Supplementary Material

Refer to Web version on PubMed Central for supplementary material.

Acknowledgments

We gratefully appreciate the technical expertise of M. Urban and G. Aguilar. We also thank O.T. Jones (University of Manchester) for the $\alpha_2\delta$-1-HA cDNA construct, and K.P. Campbell (University of Iowa) for his generous gift of the $\alpha_2\delta$-1 antibodies. This work was supported in part by a grant from The National Council for Science and Technology (Conacyt) to R.F. Doctoral and postdoctoral fellowships from Conacyt to A.C.R. and R.G.R., respectively, are gratefully acknowledged.

References

1. Berridge MJ, Lipp P, Bootman MD. The versatility and universality of calcium signalling. Nat Rev Mol Cell Biol. 2000; 1:11–21. [PubMed: 11413485]
2. Tsien RW, Lipscombe D, Madison D, Bley K, Fox A. Reflections on calcium channel diversity, 1988–1994. Trends Neurosci. 1995; 18:52–54. [PubMed: 7537405]
3. Lacinová L. Voltage-dependent calcium channels. Gen Physiol Biophys. 2005; 24(Suppl 1):1–78. [PubMed: 16096350]
4. Arikkath J, Campbell KP. Auxiliary subunits: essential components of the voltage-gated calcium channel complex. Curr Opin Neurobiol. 2003; 13:298–307. [PubMed: 12850214]
5. Felix R. Molecular regulation of voltage-gated Ca^{2+} channels. J Recept Signal Transduct Res. 2005; 25:57–71. [PubMed: 16149767]
6. Felix R. Voltage-dependent Ca^{2+} channel $\alpha_2\delta$ auxiliary subunit: structure, function and regulation. Recept Channels. 1999; 6:351–362. [PubMed: 10551267]

7. Klugbauer N, Marais E, Hofmann F. Calcium channel $\alpha_2\delta$ subunits: differential expression, function and drug binding. J Bioenerg Biomembr. 2003; 35:639–647. [PubMed: 15000524]
8. Cantí C, Nieto-Rostro M, Foucault I, Heblich F, Wratten J, Richards MW, Hendrich J, Douglas L, Page KM, Davies A, Dolphin AC. The metal-ion-dependent adhesion site in the Von Willebrand factor—a domain of $\alpha_2\delta$ subunits is key to trafficking voltage-gated Ca^{2+} channels. Proc Natl Acad Sci USA. 2005; 102:11230–11235. [PubMed: 16061813]
9. Gurnett CA, Felix R, Campbell KP. Extracellular interaction of the voltage-dependent Ca^{2+} channel $\alpha_2\delta$ and α_1 subunits. J Biol Chem. 1997; 272:18508–18512. [PubMed: 9218497]
10. Shistik E, Ivanina T, Puri T, Hosey M, Dascal N. Ca^{2+} current enhancement by α_2/δ and β subunits in *Xenopus* oocytes: contribution of changes in channel gating and α_1 protein level. J Physiol. 1995; 489:55–62. [PubMed: 8583415]
11. Bernstein GM, Jones OT. Kinetics of internalization and degradation of N-type voltage-gated calcium channels: role of the $\alpha_2\delta$ subunit. Cell Calcium. 2007; 41:27–40. [PubMed: 16759698]
12. Davies A, Douglas L, Hendrich J, Wratten J, Tran Van Minh A, Foucault I, Koch D, Pratt WS, Saibil HR, Dolphin AC. The calcium channel $\alpha_2\delta$-2 subunit partitions with $Ca_V2.1$ into lipid rafts in cerebellum: implications for localization and function. J Neurosci. 2006; 26:8748–8757. [PubMed: 16928863]
13. Robinson P, Etheridge S, Song L, Armenise P, Jones OT, Fitzgerald EM. Formation of N-type ($Ca_V2.2$) voltage-gated calcium channel membrane microdomains: lipid raft association and clustering. Cell Calcium. 2010; 48:183–194. [PubMed: 20888635]
14. Barclay J, Balaguero N, Mione M, Ackerman SL, Letts VA, Brodbeck J, Cantí C, Meir A, Page KM, Kusumi K, Perez-Reyes E, Lander ES, Frankel WN, Gardiner RM, Dolphin AC, Rees M. Ducky mouse phenotype of epilepsy and ataxia is associated with mutations in the Cacna2d2 gene and decreased calcium channel current in cerebellar Purkinje cells. J Neurosci. 2001; 21:6095–6104. [PubMed: 11487633]
15. Brill J, Klocke R, Paul D, Boison D, Gouder N, Klugbauer N, Hofmann F, Becker CM, Becker K. entla, a novel epileptic and ataxic Cacna2d2 mutant of the mouse. J Biol Chem. 2004; 279:7322–7330. [PubMed: 14660671]
16. Felix R. Insights from mouse models of absence epilepsy into Ca^{2+} channel physiology and disease etiology. Cell Mol Neurobiol. 2002; 22:103–120. [PubMed: 12363194]
17. Wycisk KA, Zeitz C, Feil S, Wittmer M, Forster U, Neidhardt J, Wissinger B, Zrenner E, Wilke R, Kohl S, Berger W. Mutation in the auxiliary calcium-channel subunit CACNA2D4 causes autosomal recessive cone dystrophy. Am J Hum Genet. 2006; 79:973–977. [PubMed: 17033974]
18. Kang MG, Felix R, Campbell KP. Long-term regulation of voltage-gated Ca^{2+} channels by gabapentin. FEBS Lett. 2002; 528:177–182. [PubMed: 12297300]
19. Vega-Hernández A, Felix R. Down-regulation of N-type voltage-activated Ca^{2+} channels by gabapentin. Cell Mol Neurobiol. 2002; 22:185–190. [PubMed: 12363200]
20. Zoidis G, Papanastasiou I, Dotsikas I, Sandoval A, Dos Santos RG, Papadopoulou-Daifoti Z, Vamvakides A, Kolocouris N, Felix R. The novel GABA adamantane derivative (AdGABA): design, synthesis, and activity relationship with gabapentin. Bioorg Med Chem. 2005; 13:2791–2798. [PubMed: 15781390]
21. Hendrich J, Van Minh AT, Heblich F, Nieto-Rostro M, Watschinger K, Striessnig J, Wratten J, Davies A, Dolphin AC. Pharmacological disruption of calcium channel trafficking by the $\alpha_2\delta$ ligand gabapentin. Proc Natl Acad Sci USA. 2008; 105:3628–3633. [PubMed: 18299583]
22. Martínez-Hernández E, Sandoval A, González-Ramírez R, Zoidis G, Felix R. Inhibition of recombinant N-type and native high voltage-gated neuronal Ca^{2+} channels by AdGABA: mechanism of action studies. Toxicol Appl Pharmacol. 2011; 250:270–277. [PubMed: 21059371]
23. Sandoval A, Oviedo N, Andrade A, Felix R. Glycosylation of asparagines 136 and 184 is necessary for the $\alpha_2\delta$ subunit-mediated regulation of voltage-gated Ca2+ channels. FEBS Lett. 2004; 576:21–26. [PubMed: 15474003]
24. Andrade A, Sandoval A, Oviedo N, De Waard M, Elias D, Felix R. Proteolytic cleavage of the voltage-gated Ca^{2+} channel $\alpha_2\delta$ subunit: structural and functional features. Eur J Neurosci. 2007; 25:1705–1710. [PubMed: 17408426]

25. Gurnett CA, De Waard M, Campbell KP. Dual function of the voltage dependent Ca^{2+} channel α_2 (subunit in current stimulation and subunit interaction. Neuron. 1996; 16:431–440. [PubMed: 8789958]
26. Douglas L, Davies A, Wratten J, Dolphin AC. Do voltage-gated calcium channel $\alpha_2\delta$ subunits require proteolytic processing into α_2 and delta to be functional? Biochem Soc Trans. 2006; 34b: 894–898.
27. Fujita Y, Mynlieff M, Dirksen RT, Kim MS, Niidome T, Nakai J, Friedrich T, Iwabe N, Miyata T, Furuichi T, Furutama D, Mikoshiba K, Mori Y, Beam KG. Primary structure and functional expression of the Ω-conotoxin-sensitive N-type calcium channel from rabbit brain. Neuron. 1993; 10:585–598. [PubMed: 8386525]
28. Castellano A, Wei X, Birnbaumer L, Perez-Reyes E. Cloning and expression of a neuronal calcium channel β subunit. J Biol Chem. 1993; 268:91, 1235, 2366.
29. Kim HL, Kim H, Lee P, King RG, Chin H. Rat brain expresses an alternatively spliced form of the dihydropyridine-sensitive L-type calcium channel α_2 subunit. Proc Natl Acad Sci USA. 1992; 89:3251–3255. [PubMed: 1314383]
30. Witcher DR, De Waard M, Sakamoto J, Franzini-Armstrong C, Pragnell M, Kahl SD, Campbell KP. Subunit identification and reconstitution of the N-type Ca^{2+} channel complex purified from brain. Science. 1993; 261:486–489. [PubMed: 8392754]
31. Scott VE, De Waard M, Liu H, Gurnett CA, Venzke DP, Lennon VA, Campbell KP. Beta subunit heterogeneity in N-type Ca^{2+} channels. J Biol Chem. 1996; 271:3207–3212. [PubMed: 8621722]
32. Liu H, Felix R, Gurnett CA, De Waard M, Witcher DR, Campbell KP. Expression and subunit interaction of voltage-dependent Ca^{2+} channels in PC12 cells. J Neurosci. 1996; 16:7557–7565. [PubMed: 8922412]
33. Hamill OP, Marty A, Neher E, Sakmann B, Sigworth FJ. Improved patch-clamp techniques for high resolution current recording from cells and cell-free membrane patches. Pflugers Arch. 1981; 391:85–100. [PubMed: 6270629]
34. Avila G, Sandoval A, Felix R. Intramembrane charge movement associated with endogenous K^+ channel activity in HEK-293 cells. Cell Mol Neurobiol. 2004; 24:317–330. [PubMed: 15206817]
35. Felix R, Gurnett CA, De Waard M, Campbell KP. Dissection of functional domains of the voltage-dependent Ca^{2+} channel $\alpha_2\delta$ subunit. J Neurosci. 1997; 17:6884–6891. [PubMed: 9278523]
36. Thompson JD, Higgins DG, Gibson TJ. CLUSTAL W: improving the sensitivity of progressive multiple sequence alignment through sequence weighting, position-specific gap penalties and weight matrix choice. Nucleic Acids Res. 1994; 22:4673–4680. [PubMed: 7984417]
37. Ferre F, Clote P. DiANNA: a web server for disulfide connectivity prediction. Nucleic Acids Res. 2005; 33:W230–W232. [PubMed: 15980459]
38. Ferre F, Clote P. DiANNA 1.1: an extension of the DiANNA web server for ternary cysteine classification. Nucleic Acids Res. 2006; 34:W182–W185. [PubMed: 16844987]
39. Kim DE, Chivian D, Baker D. Protein structure prediction and analysis using the Robetta server. Nucleic Acids Res. 2004; 32:W526–W531. [PubMed: 15215442]
40. Roy A, Kucukural A, Zhang Y. I-TASSER: a unified platform for automated protein structure and function prediction. Nat Protoc. 2010; 5:725–738. [PubMed: 20360767]
41. Klugbauer N, Lacinová L, Marais E, Hobom M, Hofmann F. Molecular diversity of the calcium channel $\alpha_2\delta$ subunit. J Neurosci. 1999; 19:684–691. [PubMed: 9880589]
42. Yasuda T, Chen L, Barr W, McRory JE, Lewis RJ, Adams DJ, Zamponi GW. Auxiliary subunit regulation of high-voltage activated calcium channels expressed in mammalian cells. Eur J Neurosci. 2004; 20:1–13. [PubMed: 15245474]
43. Kelley LA, Sternberg MJ. Protein structure prediction on the Web: a case study using the Phyre server. Nat Protoc. 2009; 4:363–371. [PubMed: 19247286]
44. Anantharaman V, Aravind L. Cache—a signaling domain common to animal Ca^{2+}-channel subunits and a class of prokaryotic chemotaxis receptors. Trends Biochem Sci. 2000; 25:535–537. [PubMed: 11084361]
45. Mascioni A, Karim C, Barany G, Thomas DD, Veglia G. Structure and orientation of sarcolipin in lipid environments. Biochemistry. 2002; 41:475–482. [PubMed: 11781085]

46. Derewenda U, Swenson L, Wei Y, Green R, Kobos PM, Joerger R, Haas MJ, Derewenda ZS. Conformational lability of lipases observed in the absence of an oil-water interface: crystallographic studies of enzymes from the fungi *Humicola lanuginosa* and *Rhizopus delemar*. J Lipid Res. 1994; 35:524–534. [PubMed: 8014587]

47. Petersen M, Johnson PH, Petersen SB. Amino acid neighbors and detailed conformational analysis of cysteines in proteins. Protein Eng. 1999; 12:535–548. [PubMed: 10436079]

48. Ellis SB, Williams ME, Ways NR, Brenner R, Sharp AH, Leung AT, Campbell KP, McKenna E, Koch WJ, Hiu A, Schwartz A, Harpold MM. Sequence and expression of mRNAs encoding the α_1 and α_2 subunits of a DHP-sensitive calcium channel. Science. 1988; 241:1661–1664. [PubMed: 2458626]

49. Jay SD, Sharp AH, Kahl SD, Vedvick TS, Harpold MM, Campbell KP. Structural characterization of the dihydropyridine-sensitive calcium channel α_2-subunit and the associated δ peptides. J Biol Chem. 1991; 266:3287–3293. [PubMed: 1847144]

50. Brickley K, Campbell V, Berrow N, Leach R, Norman RI, Wray D, Dolphin AC, Baldwin SA. Use of site-directed antibodies to probe the topography of the α_2 subunit of voltage-gated Ca^{2+} channels. FEBS Lett. 1995; 364:129–133. [PubMed: 7750557]

51. Wiser O, Trus M, Tobi D, Halevi S, Giladi E, Atlas D. The α_2/δ subunit of voltage sensitive Ca^{2+} channels is a single transmembrane extracellular protein which is involved in regulated secretion. FEBS Lett. 1996; 379:15–20. [PubMed: 8566221]

52. Hobom M, Dai S, Marais E, Lacinova L, Hofmann F, Klugbauer N. Neuronal distribution and functional characterization of the calcium channel α_2δ-2 subunit. Eur J Neurosci. 2000; 12:1217–1226. [PubMed: 10762351]

53. Gong HC, Hang J, Kohler W, Li L, Su TZ. Tissue-specific expression and gabapentin-binding properties of calcium channel α_2δ subunit subtypes. J Membr Biol. 2001; 184:35–43. [PubMed: 11687876]

54. Davies A, Kadurin I, Alvarez-Laviada A, Douglas L, Nieto-Rostro M, Bauer CS, Pratt WS, Dolphin AC. The α_2δ subunits of voltage-gated calcium channels form GPI-anchored proteins, a posttranslational modification essential for function. Proc Natl Acad Sci USA. 2010; 107:1654–1659. [PubMed: 20080692]

55. Robinson P, Etheridge S, Song L, Shah R, Fitzgerald EM, Jones OT. Targeting of voltage-gated calcium channel α_2δ-1 subunit to lipid rafts is independent from a GPI-anchoring motif. PLoS One. 2011; 6:e19802. [PubMed: 21695204]

Appendix A. Supplementary data

Supplementary data associated with this article can be found, in the online version, at doi: 10.1016/j.ceca.2011.10.002.

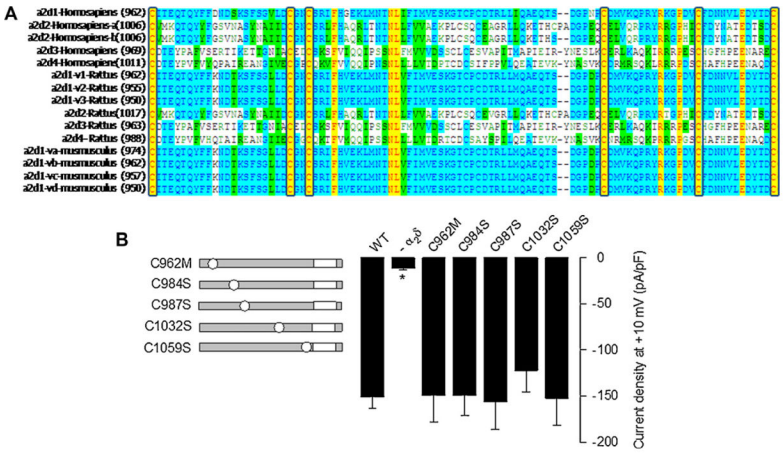

Fig. 1.

Mutation of the conserved Cys residues in the extracellular domain of the δ subunit. (A) Multiple alignment of δ proteins using Vector NTI 8 software. Sequences used were downloaded from GenBank. Residues are colored according to homology. Yellow highlights residues that are identical among species. Unshaded residues are unique, while blue and green indicate residues shared among a subset of variants or species. Sequences are from the top: human (*Homo sapiens*), rat (*Rattus norvegicus*), and mouse (*Mus musculus*). Numbers in parentheses indicate the position of the first Cys in the sequence. (B) Bar plot of current densities after a 140-ms depolarization pulse to +10 mV for the $Ca_V2.2\alpha_1/\beta_3$ recombinant channels co-expressed with the $\alpha_2\delta$-1 mutants (n = 19–131). The left panel shows a schematic representation of the point mutations in δ: gray bars represent the protein with its TM region in white. (For interpretation of the references to color in this figure legend, the reader is referred to the web version of the article.)

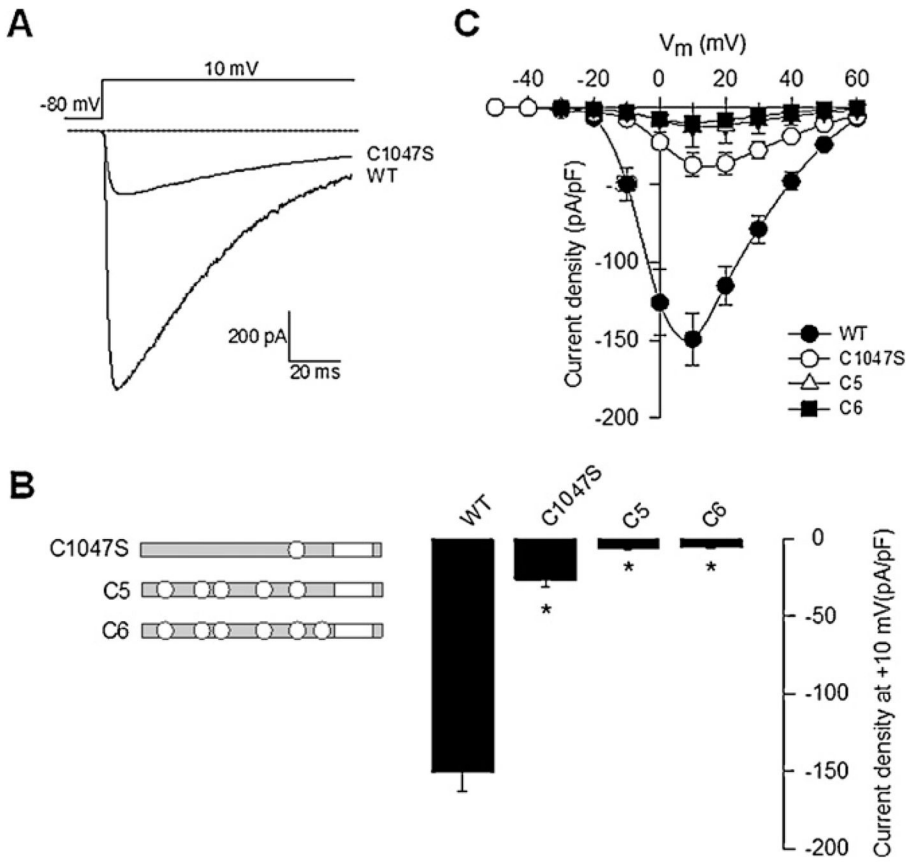

Fig. 2.

Effect of the Cys1047 residue substitution on the $\alpha_2\delta$-1 subunit function. (A) Representative macroscopic currents from HEK293 cells co-expressing $Ca_V2.2\alpha_1/\beta_3$ channels with the wild-type (WT) or the Cys1047Ser (C1047S) $\alpha_2\delta$-1 subunits during a 140-ms depolarizing pulse to +10 mV from a V_h of −80 mV. (B) Bar plot of current density after a 140-ms depolarization pulse to +10 mV for the $Ca_V2.2\alpha_1/\beta_3$ recombinant channels co-expressed with the $\alpha_2\delta$-1 mutants shown in the left as in Fig. 1B (n = 32–131). Asterisks denote statistically significant differences between WT and $\alpha_2\delta$-1 mutant subunits. (C) Average current versus voltage plots (I–V) for the $Ca_V2.2\alpha_1/\beta_3$ subunits in the presence of the $\alpha_2\delta$-1 indicated variants. Currents were evoked by 140-ms depolarizing pulses ranging from −50 mV to +60 mV in 10-mV increments from a V_h of −80 mV.

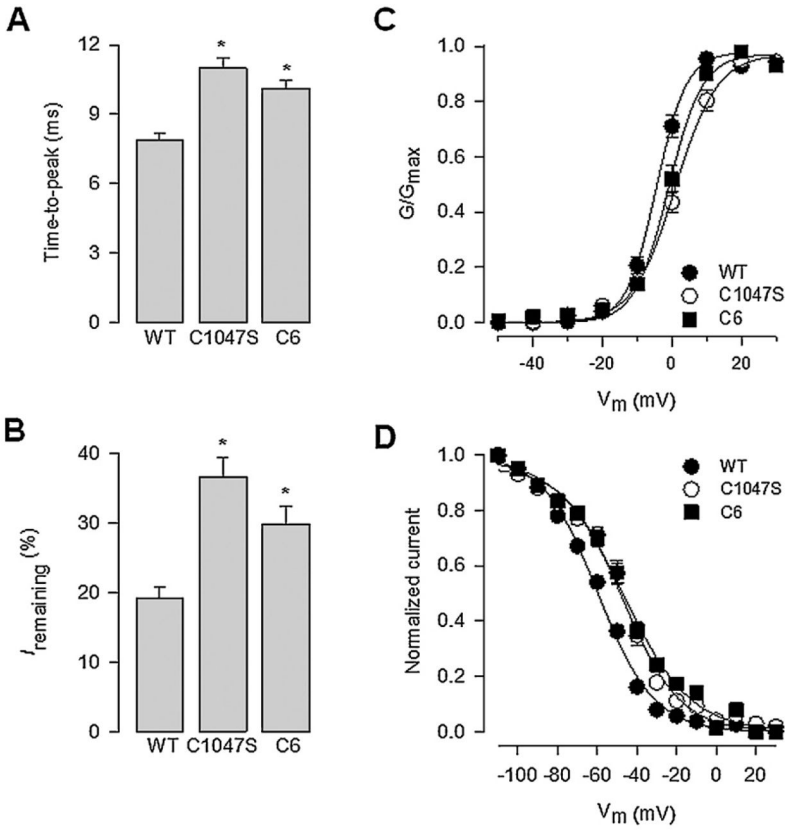

Fig. 3.

Effect of $\alpha_2\delta$-1 WT and the Cys1047 mutant proteins on the properties of the currents through N-type channels recorded in HEK293 cells. (A) Bar chart comparing current time-to-peak recorded in response to a depolarizing pulse to +10 mV from a V_h of −80 mV in cells expressing the $\alpha_2\delta$-1 WT, the Cys1047Ser or the C6 mutant subunits. (B) Proportion of non-inactivated current remaining at +10 mV in cells expressing the WT and the $\alpha_2\delta$-1 mutant subunits as listed. (C) Voltage dependence of activation of $Ca_V2.2/\beta_3$ channels co-expressed with $\alpha_2\delta$-1 WT (filled circles), the Cys1047Ser or the C6 mutant proteins (open circles and filled squares, respectively). The normalized data, obtained from recordings such as those shown in Fig. 2C, are plotted against the test pulse. Relative conductance (G/G_{max}) values were calculated and the data were fitted as described in Section 2. (D) Voltage dependence of steady-state inactivation of $Ca_V2.2/\beta_3$ channels co-expressed with $\alpha_2\delta$-1 WT (filled circles), Cys1047Ser (open circles) or the C6 mutant proteins (filled squares). Normalized data obtained from recordings such as those shown in Fig. 2C were plotted against the conditioning potentials. The mean data were fitted with a Boltzmann function.

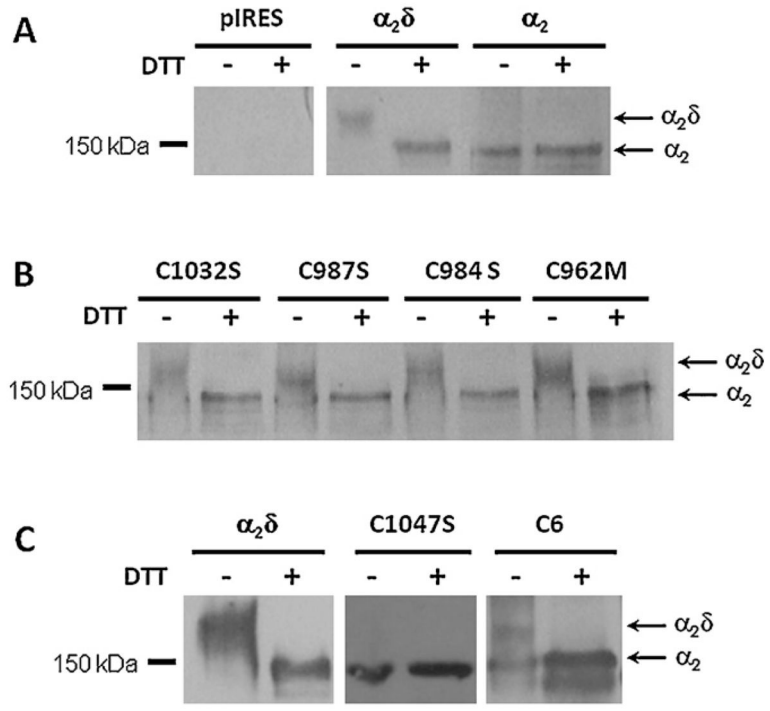

Fig. 4.

Role of Cys1047 in the formation of an intermolecular disulfide bridge in the Ca^{2+} channel $\alpha_2\delta$-1 subunit. (A) Total cell lysates from HEK293 cells transiently transfected with plasmid cDNA encoding the full length $\alpha_2\delta$-1 or the α_2 peptide were incubated with (+) or without (−) 100 mM DTT as described in Section 2. The samples were analyzed by SDS-PAGE and visualized by western blotting using the anti-$\alpha_2\delta$-1 antibodies. Cells transfected with empty vector were used as the control (pIRES). (B) Cell lysates from HEK293 cells expressing different auxiliary subunits mutated in the extracellular loop of δ were analyzed by SDS-PAGE and western blotting under reducing (+) and non-reducing (−) conditions using the same anti-$\alpha_2\delta$-1 antibodies. (C) HEK293 cells were transiently transfected with plasmid cDNA coding the $\alpha_2\delta$-1 WT and the mutant proteins Cys1047Ser and C6 and analyzed by Western blot under reducing and non-reducing conditions.

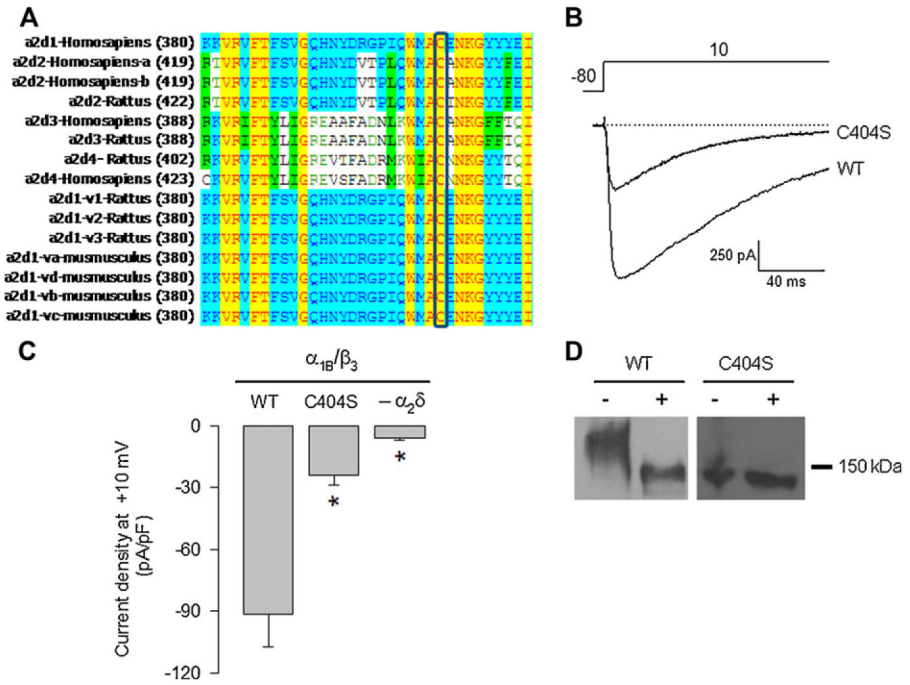

Fig. 5.

Effect of the Cys404 residue substitution on the $\alpha_2\delta$-1 subunit function and its role in disulfide bond formation. (A) Multiple alignment of different α_2 proteins. As in Fig. 1, yellow highlights residues that are identical among species, unshaded residues are unique, while blue and green indicate residues shared among variants or species. Numbers in parentheses indicate the position of the first amino acid in the sequence. (B) Superposition of representative traces to illustrate current amplitude for the subunit combinations indicated. Currents were recorded in response to a depolarizing pulse to +10 mV from a V_h of −80 mV in cells co-expressing $Ca_V2.2\alpha_1/\beta_3$ channels with the WT or the mutant (C404S) subunits. (C) Bar plot of current density after a 140-ms depolarization pulse to +10 mV for the $Ca_V2.2\alpha_1/\alpha_3$ recombinant channels expressed in the absence ($-\alpha_2\delta$-1) or the presence of the $\alpha_2\delta$-1 WT or the C404S mutant. Asterisks denote statistically significant differences with respect to the control value (WT subunit). (D) Western blot of total lysates of HEK293 cells transfected with the $\alpha_2\delta$-1 WT subunit or the C404S mutant under non-reducing or reducing conditions (− and +, respectively). (For interpretation of the references to color in this figure legend, the reader is referred to the web version of the article.)

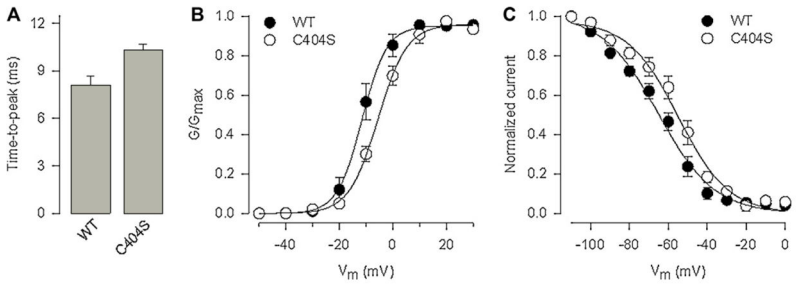

Fig. 6.

Effect of the $\alpha_2\delta$-1 Cys404 mutant protein on the properties of $Ca_V2.2/\beta_3$ (N-type) channels expressed in HEK293 cells. (A) Comparison of current time-to-peak recorded in response to a depolarizing pulse to +10 mV from a V_h of −80 mV in cells expressing the $\alpha_2\delta$-1 WT and the Cys404Ser mutant subunits. (B) Voltage dependence of activation of recombinant N-type channels co-expressed with $\alpha_2\delta$-1 WT subunit (filled circles) or the Cys404Ser mutant protein (open circles). The normalized data are plotted against the test pulse. Relative conductance (G/G_{max}) values were calculated and the data were fitted as described in Section 2. (C) Voltage dependence of steady-state inactivation of recombinant N-type channels co-expressed with $\alpha_2\delta$-1 WT (filled circles) or the Cys404Ser (open circles). Normalized data were plotted against the conditioning potentials. The mean data were fitted with a Boltzmann function.

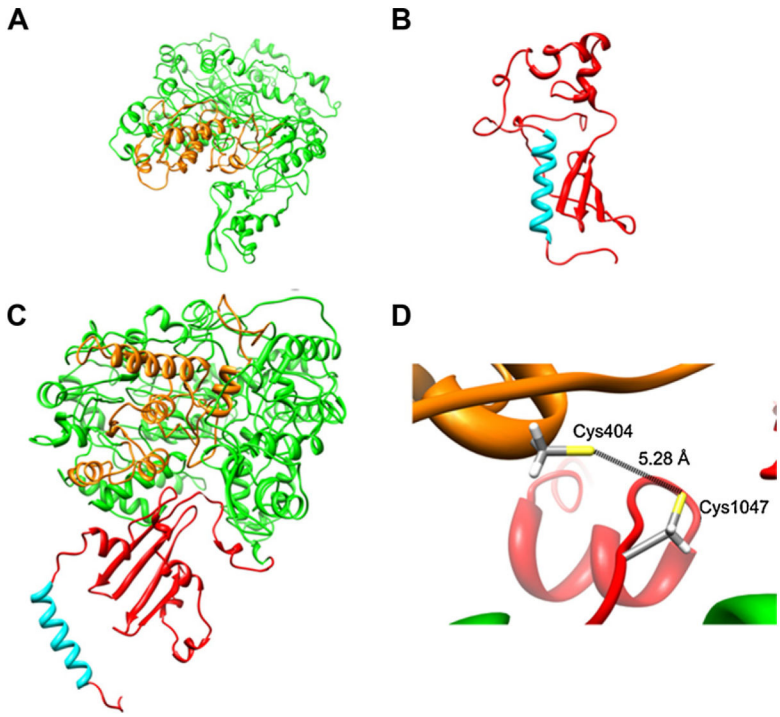

Fig. 7.

Three-dimensional model of the Ca^{2+} channel $\alpha_2\delta$-1 subunit showing the potential interaction of Cys residues at positions 404 and 1047. (A) Model of the α_2 peptide showing the vWFA domain (orange). (B) Ribbon representation of the δ peptide showing the transmembrane helix (cyan). (C) The α_2 and δ partial models were then assembled into a combined model, which was built using PDBePISA, a web-based interactive software tool widely used for prediction of probable quaternary structures. (D) Close up of the $\alpha_2\delta$-1 subunit region showing the distance between the Cys pair that participates in the proposed disulfide bridge. (For interpretation of the references to color in this figure legend, the reader is referred to the web version of the article.)